Research Article Vol. 28, No. 3 / 3 February 2020 / Optics Express 3331
Optics EXPRESS

# Reflective aperiodic multilayer filters for metrology at XUV sources

J. L. P. Barreaux,[1,*] I. V. Kozhevnikov,[2] H. M. J. Bastiaens,[1] F. Bijkerk,[3] and K.-J. Boller[1]

[1]Laser Physics and Nonlinear Optics, MESA+ Institute for Nanotechnology, University of Twente, 7500 AE Enschede, The Netherlands
[2]Shubnikov Institute of Crystallography of Federal Scientific Research Centre "Crystallography and Photonics" of Russian Academy of Sciences, Leninskiy pr. 59, Moscow 119333, Russia
[3]XUV Optics, MESA+ Institute for Nanotechnology, University of Twente, 7500 AE Enschede, The Netherlands
[*]LPNOtmw@utwente.nl

**Abstract:** We present a general method for designing XUV aperiodic multilayer mirrors that can mimic a given target spectrum, specifically, the spectral transmission of an XUV optical system. The method is based on minimizing a merit function and using fidelity parameters that quantify the matching of the multilayer reflectivity spectrum with that of the target spectrum. To assess the feasibility of fabricating such a system, we show how to reduce the layer-to-layer thickness variations throughout the aperiodic layer stack. We demonstrate the design method using an example of an EUV optical system composed of 12 identical Mo/Si multilayer mirrors having a reflectivity peak at 13.5 nm. We found that the target spectrum can be mimicked with high fidelity either with a single reflection at an aperiodic multilayer mirror combined with standard absorbing filters or, if required, with two subsequent reflections at a mimic mirror. These examples demonstrate the applicability for metrology at XUV sources, including spectrally proper source imaging. Because our approach is of general applicability, the process can be used to mimic any other narrowband, single-peaked target spectrum in the XUV region.



## 1. Introduction

The development of sources for the XUV wavelength band, typically from few tens to few tenths of a nanometer, is important for a wide range of scientific and industrial applications, such as EUV lithography [1], photoelectron spectroscopy [2], high-resolution microscopy [3], and surface analysis [4]. This development requires complex optical systems comprising of reflective multilayer mirrors for imaging, as well as dedicated XUV optical components for on-line monitoring, source metrology and standardized characterization. Specifically required are filters with an adjustable spectral shape of the transmission peak, to mimic the transmission of multi-mirror XUV optical systems with a single, reflective multilayer mirror for spectral power characterization, or, for simultaneous source imaging and brightness characterization with better out-of-band suppression, also with a dual-mirror design.

Besides absorptive filters that block wider spectral ranges, XUV monitoring and metrology is making use mainly of periodic multilayer mirrors for selective reflection [5–11] of a desired, narrowband wavelength interval. However, with periodic layers, the shape of the spectral transmission peak is fixed due to the periodicity of the layer stack. As an example, in one of our previous investigations [12], we used periodic multilayer stacks to demonstrate anomalous-transmission (AT) filters, a novel type of narrowband and wavelength-tunable XUV filter, where the spectral shape of the transmission peak is intrinsically fixed.

Here we present a general method that enables to design non-periodic XUV multilayer mirrors with the reflectivity peak having a specific spectral shape, such as for mimicking the power

#376339 https://doi.org/10.1364/OE.376339
Journal © 2020 Received 28 Aug 2019; revised 20 Dec 2019; accepted 15 Jan 2020; published 24 Jan 2020

Optics EXPRESS

transmission spectrum of an XUV imaging system that comprises multiple XUV multilayer mirrors. Based on a given transmission spectrum for the XUV optical system as target spectrum, we derive as a starting point a standard periodic multilayer stack with the same reflectivity bandwidth as that of the multi-mirror system. Thereafter, optimization of the spectral shape is carried out with a numerical method. The method involves defining three essential design criteria that quantify the similarity of the multilayer stack reflectivity spectrum with the target spectrum. We show that the optimization yields the design of an aperiodic multilayer mirror that mimics the target spectrum with high fidelity both in single or dual reflection. In order to facilitate fabrication using a reduced layer thickness variation throughout the layer stack, we show how to minimize the layer-to-layer thickness variations with additional numerical optimization.

Our approach is of general applicability in that it can be used to mimic the throughput of any XUV optical system with a narrowband (single-peaked) and smooth spectrum. Referring to EUV lithography (EUVL), we demonstrate the design of aperiodic multilayer mirrors that mimic the transmission of a 13.5-nm optical system of multiple Mo/Si mirrors. While the main body of this paper is dedicated to the theoretical approach to the design of such a mimic mirror, considerations related to experimental and fabrication issues are made in Appendix A.

## 2. Fidelity parameters and merit function

Complete throughput specifications of actual EUVL optical systems are not publicly available. Therefore, we select an arbitrary multimirror optical system of high complexity [13], and chose as the target spectrum the reflective throughput of 12 subsequent, identical Mo/Si multilayer mirrors that are optimized for maximum reflectivity at 13.5 nm [14,15].

In Fig. 1 we show on a logarithmic scale the experimental reflectivity of a single, high-performance periodic Mo/Si multilayer mirror (curve 1, [16]), normalized to its peak value at the center wavelength, $\lambda_0$ (69.8% at 13.5 nm). The reflectivity spectrum shows a bandwidth (full-width at half maximum, FWHM) of about $\delta\lambda/\lambda = 4\%$. The target spectrum we chose to mimic is displayed as curve 2, which is the $12^{\text{th}}$ power of the single-mirror experimental reflectivity, to represent reflection in an optical system with twelve such mirrors. The resulting spectrum, see curve 2, shows a clearly reduced bandwidth of about 2%. Outside this target Bragg peak, the reflectivity decreases steeply to extremely low values, at least 5 orders of magnitude lower than in the single-mirror spectrum. Having a low reflectivity across a wide range around the reflection peak is of high importance because the spectrum of current high-power EUV sources is in principle broadband. Spanning from the soft X-ray range into the infrared (IR) region, a large amount of radiation would otherwise be reflected in undesired wavelength ranges as so-called out-of-band radiation.

Having to provide such extremely low target reflectivity with a single mimic mirror is actually a fundamental problem, because such low reflectivity can only be provided, if possible at all, across limited spectral intervals. More specifically, depending on their design, multilayer mirrors can certainly suppress the reflection of a range of XUV wavelengths. However, at longer wavelengths, from the ultraviolet to IR range, there will remain an undesired, higher reflectivity, because the polarizability of all materials grows towards longer wavelength.

A standard method for broadband blocking longer wavelengths is to employ absorbing transmission filters in addition. Here we will make use of the same method, i.e., we aim on designing mimic multilayer mirrors that are to be used in sequence with an absorbing filter that blocks the long-wavelength tail of radiation. In the following we term such combination of the mimic mirror with an absorption filter the mimic optical system.

In order to quantify how closely the target spectrum is reproduced with a mimic optical system, we introduce the following three fidelity parameters that emphasize the most important spectral

Optics EXPRESS

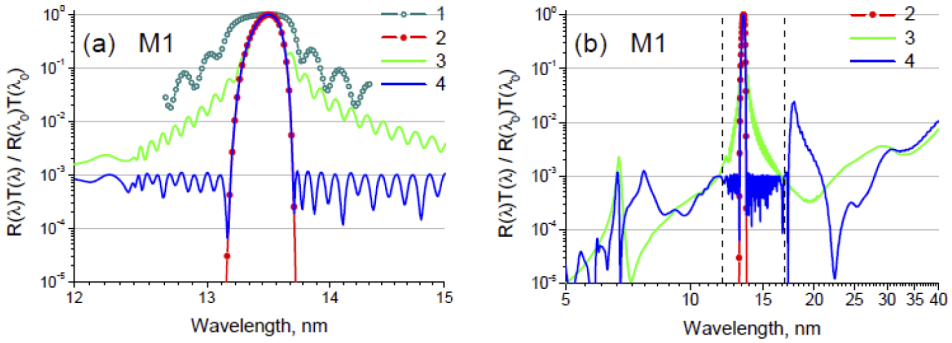


**Fig. 1.** EUV reflectivity spectra normalized to unity at 13.5 nm for direct comparison of the spectral shapes and presented in the vicinity of the Bragg peak (a) and across a wider spectral interval (b). *Curve 1*: experimental reflectivity spectrum of a single Mo/Si periodic multilayer mirror optimized for maximum reflectivity (68.9% [16]) at a wavelength of 13.5 nm. *Curve 2*: target reflectivity curve to be mimicked, calculated as the reflectivity after 12 subsequent reflections off the experimental Mo/Si mirror. *Curve 3*: reflectivity of periodic $MoSi_2$/Si mirror. *Curve 4*: reflectivity of an aperiodic $MoSi_2$/Si mirror (mirror M1) with the bi-layer thickness depth-distribution shown in Fig. 2. The vertical dashed lines indicate the optimization interval.

properties of the mimicking:

$$\chi_1 = \frac{\int_{OP} \rho(\lambda)\,\mathrm{d}\lambda}{\int_{IP} \rho(\lambda)\,\mathrm{d}\lambda}; \qquad \chi_2 = \left[\int_{IP} \frac{(\rho(\lambda)-\rho_0(\lambda))^2}{\rho_0(\lambda)} \frac{\mathrm{d}\lambda}{\Delta\lambda}\right]^{1/2}; \qquad \chi_3 = \max_{OP} \rho(\lambda); \tag{1}$$

$$\rho(\lambda) = \frac{R(\lambda)}{R(\lambda_0)} \cdot \frac{T(\lambda)}{T(\lambda_0)}; \qquad \rho_0(\lambda) = \frac{R_0(\lambda)}{R_0(\lambda_0)}; \qquad \lambda_0 = 13.5\ \text{nm}. \tag{2}$$

In these expressions, $R_0(\lambda)$ is the target reflectivity of the optical system to be mimicked (here a sequence of reflection at 12 Mo/Si mirrors), and $\Delta\lambda$ is the spectral width (FWHM) of the target Bragg peak. $R(\lambda)$ is the reflectivity of the mimic mirror and $T(\lambda)$ is the transmittance of an additional, broadband absorption filter. We note that $R(\lambda)$ in Eq. (2) can be replaced by $(R(\lambda))^n$ if not only the target spectrum has to be mimicked, but if spectral mimicking has to be carried out with a source-imaging telescope that comprises a number of $n$ mimic mirrors, such as characterizing the brightness of XUV sources. Such source imaging can be done most effectively with two subsequent mimic mirrors ($n = 2$, i.e. dual reflection), a broadband absorption filter, and a spatially resolving detector [14,15]. The values of $R$, $T$, and $R_0$ are normalized to those at the center wavelength (here $\lambda_0 = 13.5$ nm) where the target reflectivity is highest. Integration in Eq. (1) is performed either inside the target peak (*IP*, considering all in-band radiation) or outside the target peak (*OP*, out-of-band radiation).

The first parameter, $\chi_1$, determines the spectral purity of the beam after transmission through the mimic optical system, i.e., the ratio of the in-band radiation power to that of undesirable out-of-band radiation. The second parameter, $\chi_2$, characterizes an averaged relative deviation from the target reflectivity peak. The third parameter, $\chi_3$, characterizes the maximum transmittance value of the mimic optical system anywhere outside the target reflectivity peak.

We note that minimizing only single fidelity parameters is insufficient for obtaining a high-quality mimic system. For instance, minimizing $\chi_1$ cannot guarantee the absence of narrow but high reflectivity peaks outside of the desired spectral range, which would be unacceptable in most applications. An optimum mimic filter needs to provide minimum values for all three fidelity parameters simultaneously, noting that these conditions might be mutually exclusive.

Optics EXPRESS

In addition to the fidelity parameters, the factor $R(\lambda_0)T(\lambda_0)$ characterizes the peak (center wavelength) transmission of the mimic optical system, which should be high enough for practical applications. Given the extremely high output power of current EUV sources, a smaller transmittance of several percent can be considered as well sufficient for spectral monitoring, metrology and standardized characterization.

We solve the designing problem by using a numerical approach based on the minimization of the following merit function:

$$MF = \frac{1}{M_{IP}} \sum_{IP} \left[ \frac{\rho(\lambda_j) - \rho_0(\lambda_j)}{\rho_0(\lambda_j)} \right]^2 + \frac{Q}{M_{OP}} \sum_{OP} \left[ \frac{\rho(\lambda_j) - \rho_{max}}{\rho_{max}} \right]^2 u_j, \quad \text{where } u_j = \begin{cases} 0, \text{ if } \rho(\lambda_j) < \rho_{max} \\ 1, \text{ otherwise} \end{cases}. \tag{3}$$

The summation in Eq. (3) is performed over two sets of wavelengths, $M_{IP}$ wavelengths inside the target Bragg peak and $M_{OP}$ outside the peak. The first term in Eq. (3) is the in-band mean-square deviation between the mimic and target reflectivity peaks. The second term is introduced to obtain low total transmittance $\rho(\lambda)<\rho_{max}$ from the mimic outside the target peak, where $\rho_{max}$ is a threshold parameter to be chosen before the start of the optimization procedure. The width of the Bragg peak, $\Delta\lambda$ in Eq. (1), is measured at this threshold level, where $\rho_0(\lambda) = \rho_{max}$, and the second sum is multiplied with the function $u_j$ (zero if $\rho(\lambda_j)<\rho_{max}$). This approach makes the optimization process much easier, by letting the minimization algorithm ignore contributions where the mimic transmittance $\rho(\lambda)$ is less than the chosen threshold, $\rho_{max}$. Finally, the relative weight of the first and second term in the merit function can be adjusted with the parameter $Q$. Increasing $Q$ puts more emphasis on lowering the reflectivity down to $\rho_{max}$ outside the Bragg peak, while decreasing $Q$ imposes a closer convergence to the target reflectivity inside the peak.

When minimizing the merit function, we use the plane wave approximation for calculating the reflectivity spectrum $R(\lambda)$, and we neglect fabrication-related errors such as deviations in optical constants, layer thicknesses or surface roughness. A discussion of the influence of these effects on the mimic mirror performance in terms of the fidelity parameters is given in Appendix A. It turns out that the mimic mirror reflectivity shows high robustness vs random deviations, and that systematic deviations can be compensated, e.g., with a slight change of the angle of incidence.

As the starting point for the algorithm, we use a periodic multilayer mirror with a 2% reflectivity bandwidth, same as for the target spectrum, which simplifies the optimization procedure. Note that the spectral width of the reflectivity peak is proportional to the value of $|\Delta\varepsilon| \cdot \sin(\pi\Gamma)$, where $\Delta\varepsilon$ is the difference of the dielectric constants of the two selected mirror materials, and where $\Gamma = d_A/d$ is the ratio between the thickness of the heavy element (absorber) layers, $d_A$, and the multilayer period, $d$. The first step in designing mimic mirrors, either for single or dual reflection, is choosing an appropriate absorber material, to be combined with Si as the light (spacer) material, in order to provide the necessary reflectivity bandwidth (2% here). Although pure molybdenum is often considered as absorber material for the intended wavelength of 13.5 nm, it turns out that attaining a bandwidth of 2% with a single mimic mirror layer stack would require a very small thickness ratio $\Gamma$. The corresponding Mo layers would have to be thinner than 1.5 nm, which leads to technological problems in fabrication. Specifically, the deposition of Mo/Si multilayers involves a formation of molybdenum silicide interlayers of considerable thickness (0.6–0.8 nm) and unknown density [17,18], which would lead to uncontrolled optical material properties.

To mitigate such technological problems, we chose to design a $MoSi_2$/Si multilayer mimic mirror instead, where $MoSi_2$ is the spacer material. The first advantage is that this leads to sharp and stable interfaces, because $MoSi_2$ and Si are neighbors in the phase diagram of Mo-Si alloys and, thus, are close to thermodynamic equilibrium. The second advantage is a high thermal stability with invariable reflectivity up to the annealing temperature of 1000 K, instead of 600 K

Optics EXPRESS

for conventional Mo/Si structure [19]. This is important for mirrors operating under high thermal and radiation loads. The third advantage is that, at 13.5 nm wavelength, the difference between the dielectric constants of $MoSi_2$ and Si is about a factor of two smaller than between pure Mo and Si. This reduces the spectral width of the reflectivity peak by the same factor and thereby assists mimicking the narrow bandwidth of optical systems based on multiple reflections from Mo/Si mirrors.

As the starting point of the optimization with the peak reflectivity at a wavelength of 13.5 nm, we determine a periodic $MoSi_2$/Si mirror with layer thicknesses of 2.4 and 4.4 nm for $MoSi_2$ and Si, respectively ($d$ = 6.8 nm and $\Gamma$ = 0.35), number of bi-layers $N$ = 100.5 (201 layers) and the uppermost and lowermost layers of the structure being silicon. The chosen number of bi-layers is quite practicable from technological point of view and, as it will be demonstrated below, allows mimicking the target spectrum with high accuracy. The reflectivity of the $MoSi_2$/Si periodic mirror is rather high and achieves 52.3% at the center wavelength. For taking into account the formation of a natural oxidation layer after fabrication, we assume that a 1.5 nm thick $SiO_2$ oxide layer is present on top of the mirror stack. The substrate material is taken as fused quartz.

For calculating the reflectivity spectra of multilayer structures, we make use of the optical constants of materials as provided in the CXRO X-Ray Database [20]. Typically we impose a limitation on the minimal layer thickness of $d_{min}$ = 1 nm, as to comply with the technological possibilities of depositing smooth continuous film. The angle of incidence is set to 10° from the surface normal, with the incident radiation being unpolarized.

For the optimization procedure, the fitting parameters are the thicknesses of all the 201 $MoSi_2$ and Si layers. Minimizing the merit function is performed using the standard Levenberg-Marquardt algorithm [21]. We note that the merit function possesses a large number of local minima, which raises the question of convergence. However, using a Levenberg-Marquardt algorithm, without any additional conditions, simply by using as the initial guess a periodic ML mirror with similar central wavelength and spectral bandwidth, is what enables convergence to practical solutions that are attractive for meeting the typical requirements of a mimic mirror design. The number of wavelengths inside and outside the reflectivity peak in Eq. (3) is typically set to $M_{IP}$ = 30 and $M_{OP}$ = 180, and the parameter $Q$ value was typically varied in the range from 0.1 to 5.0. As will be shown below, such a choice for the parameters $N$, $Q$, $M_{IP}$, and $M_{OP}$ allows to fit the target peak with high accuracy while achieving low reflectivity outside of the peak.

## 3. Design of aperiodic mimic mirrors for single reflection

In the following, we describe the design of a series of eight filters to be used in single reflection, starting with a simplistic approach, followed by several steps of refinement. Presenting the results progressively aims on revealing the central physical arguments more clearly, i.e., which design detail cause which contributions to the spectra, and which trade-off considerations play a role.

We begin by designing a first mimic mirror (termed M1), simply by minimizing the merit function in a somewhat narrower range of 12–17 nm, choosing a threshold reflectivity parameter of $\rho_{max} = 10^{-3}$. In this calculation, no limitation was imposed on the individual layer thickness, and an additional transmission filter for blocking radiation at longer wavelengths was not considered (i.e., $T(\lambda) = 1$ in Eq. (2)). The resulting distribution of the layer thickness vs. depth in the stack is presented in Fig. 2 (M1) while the mirror reflectivity in the 12 to 15 nm range is shown in Fig. 1, curve 4. Here and below we present the reflectivity in a narrow spectral interval (Fig. 1(a)) to show the accuracy of the target reflectivity peak fitting, and in a wide spectral region (Fig. 1(b)) to demonstrate the low transmittance of a mimic system outside the central peak. The optimization interval is indicated by vertical dashed lines. For comparison, the target reflectivity (curve 1) and the reflectivity of the periodic $MoSi_2$/Si mirror (curve 2) are also shown. It can be seen that the reflectivity peak of the mimic mirror matches almost identically the reflectivity peak of the target spectrum. Outside of the peak, the reflectivity of the mimic mirror drops sharply by three orders

Optics EXPRESS

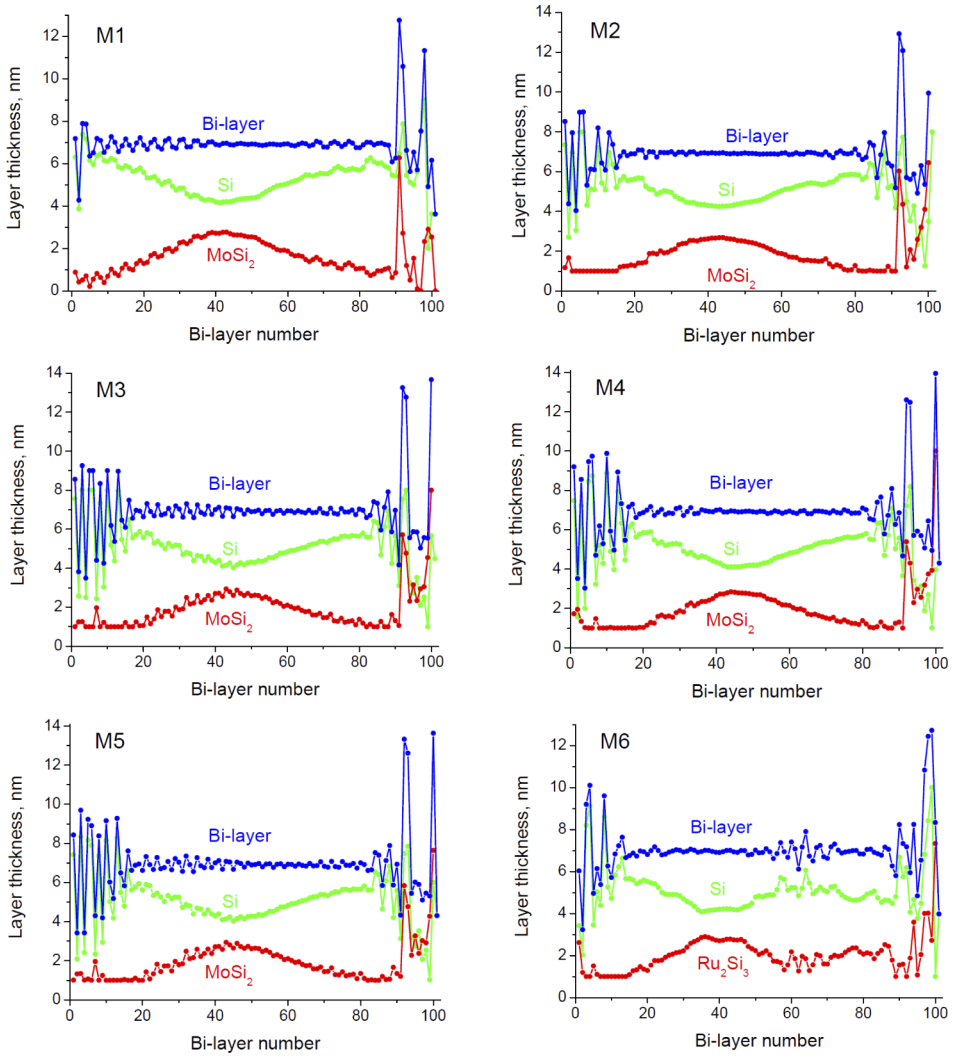


**Fig. 2.** Distributions of layer thickness for various mimic multilayer mirrors obtained via numerical optimization with different limitations on optimization parameters. The bi-layer number is counted from the top of the mirror. The natural $SiO_2$ layer and Si substrate taken into account in the calculations are not displayed.

of magnitude as required via the according setting of $\rho_{max}$. Quite differently, the periodic mirror displays up to two orders of magnitude higher reflectivity.

The main problem when designing the mimic mirror is to decrease sharply the reflectivity outside of the Bragg peak. The computational algorithm provides convergence towards a low off-band reflectivity by introducing quasi-periodic variations in the thickness of the layers within the top and bottom of the multilayer structure. At the center of the multilayer structure, the bi-layer thickness remains almost constant to provide a high reflectivity peak with matching shape. One can actually notice that all the multilayer stacks presented in Fig. 2 are approximately periodic, and thus share some coarse similarity. The similarity is simply due to the similarity of the target spectra, which comprise, as their dominant feature, a single, relatively narrowband peak at the same center wavelength. However, the layer thickness oscillations within the top and

Optics EXPRESS

the bottom cause oscillations also in the bi-layer thickness, with values that differ greatly from that of the initial, periodic structure. As a result, the reflectivity of the mimic mirrors tends to increase outside of the peak. If such an increase in reflectivity outside of the peak starts to exceed the chosen threshold parameter, $\rho_{max}$, the optimization introduces new oscillations of larger amplitude in the layer thickness depth-distribution. Unfortunately, this leads to the appearance of undesired reflectivity peaks beyond the long-wavelength side of the chosen optimization interval (see Fig. 1(b), curve 4, outside the range from 12 to 17 nm). These parasitic reflectivity peaks are not a shortcoming of the optimization algorithm but are a fundamental property of interference in multilayer systems.

This clearly shows the need to employ absorptive transmission filters in addition to mimic mirrors, in order to suppress long-wavelength parasitic reflectivity peaks. It can be expected that selecting a most suitable filter is to be included into the optimization of the mimic mirror design (via $T(\lambda)$ in Eq. (2)). Specifically, filter materials with different absorption spectra and thickness have to be discussed, and the feasibility (fabrication and stability of thin absorbing membranes) of an absorptive filter must be considered.

A second, well-known issue in optimizing multilayer mirrors stacks can be identified with M1 as well. It can be seen that the thicknesses of the $MoSi_2$ layers near the top and bottom of the stack are extremely thin, only a fraction of a nanometer. To arrive at more feasible designs, it is required to impose a limitation on the optimization parameters, which is a minimum allowed layer thickness, $d_{min}$.

To investigate the effects of an additional absorption filter and a limitation on the lowest layer thickness, we present the following two designs, M2 and M3. For the absorption filter, we begin with a technologically simple choice in the form of a free-standing $Si_3N_4$ membrane with an appreciable thickness of 250 nm. This choice is straightforward for an experimental implementation, because free-standing $Si_3N_4$ membranes are highly stable and commercially available with thicknesses as low as 50 nm (Silson Ltd.). The transmittance of the $Si_3N_4$ membrane (Fig. 3) becomes progressively lower as desired beyond a wavelength of 17 nm, where parasitic peaks had occurred with M1.

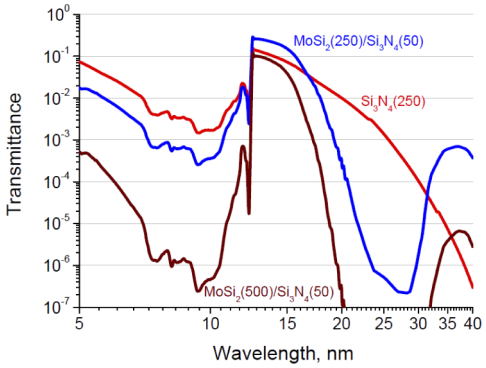


**Fig. 3.** The spectral transmittance of several free-standing absorbing filters used in our calculations. The numbers between brackets indicate the layer thickness in nm.

In expectation of absorptive suppression at longer wavelengths, for M2 we slightly extended the optimization wavelength interval towards the long-wavelength side ($\rho_{max} = 10^{-3}$ from 12 to 20 nm), and for M3 we slightly lowered the threshold parameter ($\rho_{max} = 3 \cdot 10^{-4}$ from 12-20 nm). As the starting point, the same $MoSi_2$/Si periodic multilayer structure as for M1 was used. A minimum layer thickness of $d_{min} = 1$ nm was introduced, which is a typical value beyond which smooth continuous layers can usually be fabricated.

Optics EXPRESS

Figure 2 shows the depth distributions of layer thickness for M2 and M3 as obtained from the optimization algorithm, and the corresponding total transmission spectra, $R(\lambda)T(\lambda)$, are shown in Figs. 4 and 5, respectively. When compared with M1, the depth-distributions of layer thickness are more complex and show oscillations with even larger amplitudes. Another observation is that, despite the introduction of the absorbing filter and the widening of the spectral interval of optimization, we still observe an increase in total transmittance in the long-wavelength range, beyond the end of the optimization interval ($\lambda$>20 nm). Finally, M3 exhibits a much higher parasitic reflectance peak than M2, which shows that simply lowering the threshold reflectivity leads to lower performance elsewhere in the spectrum. The increased parasitic reflectance of M3 at long wavelengths can be associated with the more pronounced oscillations in the layer thickness for M3 when compared to that for M2.

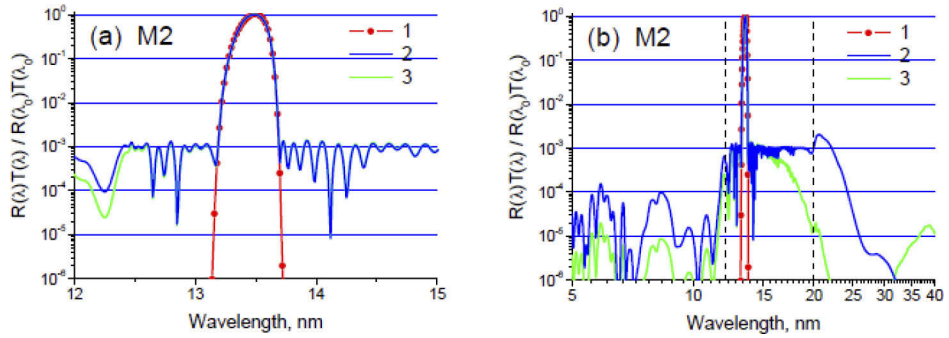


**Fig. 4.** Total transmittance versus wavelength shown near the Bragg peak (a) and in a wider spectral interval (b) of the optical systems consisting of the multilayer mirror M2 combined with a $Si_3N_4$ (250 nm) (*curve 2*) or a $MoSi_2/Si_3N_4$ (250/50 nm) (*curve 3*) free-standing absorbing filter. *Curve 1* is the target reflectivity. The vertical dashed lines indicate the optimization interval.

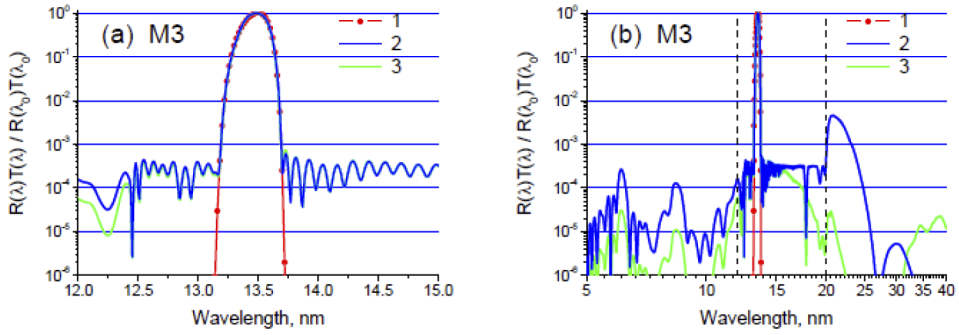


**Fig. 5.** Total transmittance versus wavelength shown near the Bragg peak (a) and in a wider spectral interval (b) of the optical systems consisting of the multilayer mirror M3 combined with a $Si_3N_4$ (250 nm) (*curve 2*) or a $MoSi_2/Si_3N_4$ (250/50 nm) (*curve 3*) free-standing absorbing filter. *Curve 1* is the target reflectivity. The vertical dashed lines indicate the optimization interval.

From the results of M2 and M3, it can be seen that the 250 nm thick $Si_3N_4$ transmission filter is unable to suppress the parasitic peak. Indeed, as can be seen in Fig. 3, the transmittance of this filter decreases rather slowly, by only one order of magnitude for increasing wavelength from 13.5 nm to 20 nm, which is insufficient for suppressing effectively the parasitic peak. Of course, it would be possible to increase the thickness of the absorbing $Si_3N_4$ layer, by a factor

Optics EXPRESS

of three for instance, resulting in the transmittance being reduced by three orders of magnitude at the 20 nm wavelength, enough to suppress efficiently the parasitic peak, even for the mirror M3. However, the filter transmittance at the 13.5 nm wavelength would be also reduced by the same three orders of magnitude, down to $10^{-4}$, which is impracticable. Therefore, it is necessary to use a different filter material demonstrating a much quicker decrease in transmittance, i.e., an increase in absorption, for increasing wavelength from 13.5 to 20 nm. According to the optical constants available in the CXRO X-Ray Database [20], the most suitable material would be molybdenum, whose absorptivity increases by three orders of magnitude in the spectral interval considered and is lower than that of $Si_3N_4$ at the 13.5 nm wavelength. Instead of using pure Mo for the transmission filter, we consider using $MoSi_2$, as it also allows to decrease, in addition, the transmittance below the absorption edge of silicon ($\lambda$<12.4 nm). We are not aware of any attempt to fabricate a free-standing $MoSi_2$ membrane of submicron thickness, however, another possibility is to deposit the $MoSi_2$ film onto the free-standing $Si_3N_4$ membrane. As an example, we have successfully deposited in a previous work a Ni/Si multilayer structure of about 500 nm total thickness onto a 50 nm thick membrane without disrupting it [12]. The spectral transmittance of a combined $MoSi_2/Si_3N_4$ (250/50 nm) transmission filter is shown in Fig. 3 (blue curve).

By replacing the $Si_3N_4$ absorbing filter used with mirrors M2 and M3 for the combined $MoSi_2/Si_3N_4$ (250/50 nm) filter, we observe that the parasitic peak at $\lambda$>20 nm is effectively suppressed, as shown in Fig. 4 and Fig. 5, curves 3. The fidelity parameters for the mirrors M2 and M3 in this configuration are summarized in Table 1. As can be seen, the spectral purity of the outgoing radiation, determined by the parameter $\chi_1$, is relatively high: the out-of-band radiation power contributes only 1.5% (M2) or 0.54% (M3) to the system throughput. The rms-deviation of the calculated reflectivity peak from the target one is 3 to 6%, with the extremely low transmittance of the peak edges contributing mainly to the $\chi_2$ value. Therefore, these optical systems seem quite suitable for practical applications.

**Table 1. Fidelity parameters of mimic optical systems consisting of aperiodic multilayer mirrors and free-standing absorbing filters.**

| | Mirror | Absorbing filter | $\rho_{max}$ | $R_0$ | $T_0$ | $R_0T_0$ | $\chi_1$ | $\chi_2$ | $\chi_3$ |
|---|---|---|---|---|---|---|---|---|---|
| M2 | $MoSi_2$/Si | $MoSi_2$ (250 nm)/ $Si_3N_4$ (50 nm) | $1 \cdot 10^{-3}$ | 0.36 | 0.24 | 0.086 | $1.5 \cdot 10^{-2}$ | $2.8 \cdot 10^{-2}$ | $1.5 \cdot 10^{-3}$ |
| M3 | $MoSi_2$/Si | $MoSi_2$ (250 nm)/ $Si_3N_4$ (50 nm) | $3 \cdot 10^{-4}$ | 0.34 | 0.24 | 0.081 | $5.4 \cdot 10^{-3}$ | $4.2 \cdot 10^{-2}$ | $7.5 \cdot 10^{-4}$ |
| M4 | $MoSi_2$/Si | $MoSi_2$ (250 nm)/ $Si_3N_4$ (50 nm) | $3 \cdot 10^{-4}$ | 0.33 | 0.24 | 0.077 | $6.9 \cdot 10^{-3}$ | $3.2 \cdot 10^{-2}$ | $5.2 \cdot 10^{-4}$ |
| M5 | $MoSi_2$/Si | $MoSi_2$ (500 nm)/ $Si_3N_4$ (50 nm) | $1 \cdot 10^{-4}$ | 0.33 | 0.087 | 0.029 | $1.8 \cdot 10^{-3}$ | $5.7 \cdot 10^{-2}$ | $2.9 \cdot 10^{-4}$ |
| M6+M6 | $Ru_2Si_3$/Si | $MoSi_2$ (300 nm)/ $Si_3N_4$ (50 nm) | $1 \cdot 10^{-6}$ | 0.16 | 0.19 | 0.031 | $3.7 \cdot 10^{-5}$ | $5.3 \cdot 10^{-2}$ | $1.6 \cdot 10^{-6}$ |
| M7 | $MoSi_2$/Si | $MoSi_2$ (250 nm)/ $Si_3N_4$ (50 nm) | $1 \cdot 10^{-3}$ | 0.38 | 0.24 | 0.090 | $1.9 \cdot 10^{-2}$ | $5.8 \cdot 10^{-2}$ | $1.4 \cdot 10^{-3}$ |
| M8 | $MoSi_2$/Si | $MoSi_2$ (250 nm)/ $Si_3N_4$ (50 nm) | $1 \cdot 10^{-3}$ | 0.37 | 0.24 | 0.089 | $2.3 \cdot 10^{-2}$ | $5.3 \cdot 10^{-2}$ | $2.4 \cdot 10^{-3}$ |

Next, we worked on decreasing further the total transmittance of the mimic filter outside the Bragg peak, by using the mirrors M2 and M3 as an initial design for the optimization process and by setting the value of $\rho_{max}$ to $3 \cdot 10^{-4}$ and $1 \cdot 10^{-4}$, respectively. The optimization in the first case, using M2 and $\rho_{max} = 3 \cdot 10^{-4}$, yields the mirror M4, whose structure is similar to that

Optics EXPRESS

of M2 but with slightly increased amplitude of layer oscillations near the top of the mirror (see Fig. 2). The total transmittance of the system consisting of the mirror M4 combined with the $MoSi_2/Si_3N_4$ (250/50 nm) absorbing filter is shown in Fig. 6, curve 2. The fidelity parameters (Table 1) are close to those of the mirror M3 operating with the same absorbing filter.

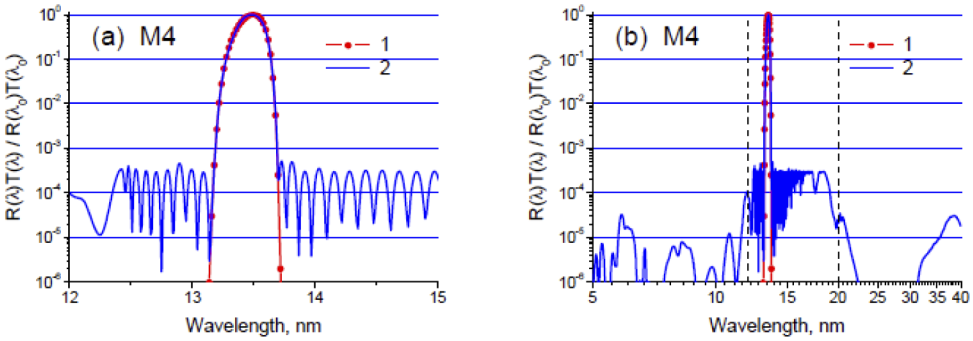


**Fig. 6.** Total transmittance versus wavelength shown near the Bragg peak (a) and in a wider spectral interval (b) of the optical systems consisting of the multilayer mirror M4 combined with a $MoSi_2/Si_3N_4$ (250/50 nm) (*curve 2*) free-standing absorbing filter. *Curve 1* is the target reflectivity. The vertical dashed lines indicate the optimization interval.

In order to design a mirror with the extremely low value $\rho_{max} = 1 \cdot 10^{-4}$, it was necessary to increase the thickness of the $MoSi_2$ layer in the absorbing filter up to 500 nm. The transmittance of a $MoSi_2/Si_3N_4$ (500/50 nm) absorbing filter is shown in Fig. 3 (brown curve), exhibiting a much narrower peak and lower transmittance for $\lambda$>20 nm. This leads the function $u_j$ in the merit function (Eq. (3)) to ignore sums over a wider wavelength range, i.e., the wavelength optimization range becomes narrower. The resulting mirror M5 has a layer thickness distribution almost identical to that of the mirror M3, while a slight increase in layer oscillations can be observed near the top of the multilayer structure (see Fig. 2). At the same time, the total transmittance outside the Bragg peak (parameter $\chi_1$) of the system consisting of the mirror M5 and the $MoSi_2/Si_3N_4$ (500/50 nm) absorbing filter is decreased by a factor of three as compared with the M3 system (see Table 1), so that the contribution of out-of-band radiation to the total throughput is only 0.18%. However, the peak transmittance at $\lambda$ = 13.5 nm is also decreased down to 2.9%, as compared to 8.3% for the M3 system. The total transmittance of the M5 mirror combined with the transmittance filter is shown in Fig. 7, curve 2.

A particularity of the mirror M5 is illustrated in Fig. 8, where the absolute values of the reflectivity of mirrors M2 and M5 without absorbing filter are shown versus the wavelength (curves 1 and 2). For comparison, the absolute values of the reflectivity of a single $MoSi_2$-Si interface (curve 3) and of an uncoated fused silica substrate (curve 4) are also shown. As can be seen, the reflectivity of the mirror M2 ($\rho_{max} = 1 \cdot 10^{-3}$) outside of the peak follows that of a single $MoSi_2$-Si interface. Decreasing the value of $\rho_{max}$ down to $1 \cdot 10^{-4}$ has resulted in mirror M5, whose reflectivity is an order of magnitude lower than that of an uncoated substrate in a rather wide spectral interval, i.e., the mirror M5 acts like an antireflective filter with respect to an uncoated substrate. Most likely, this is one of the first examples where an antireflective filter in a rather wide spectral interval is a desired feature for EUV optics. The figure offers also some insight into the problems of designing a mimic mirror with extremely low reflection of out-band radiation ($\rho_{max}<1 \cdot 10^{-3}$).

With mirrors M1 to M5, we have demonstrated the possibility to design mimic mirrors operating together with transmitting filters and providing strong suppression of out-band radiation, whose contribution to the detected signal is less than 1%, achieving a low 0.18% for the mimic mirror M5.

Optics EXPRESS

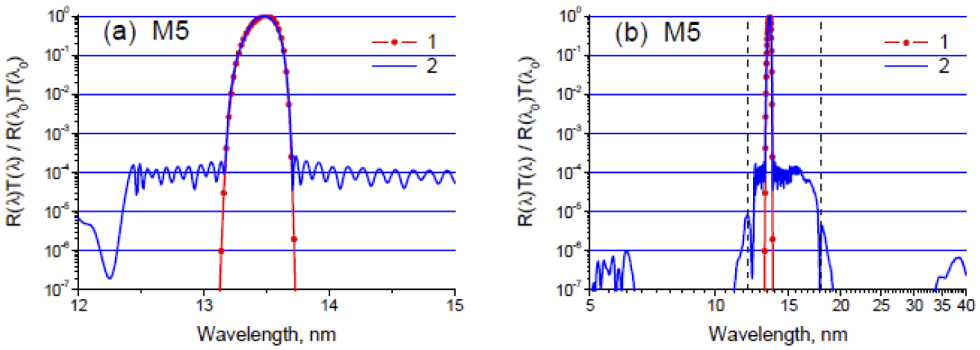


**Fig. 7.** Total transmittance versus wavelength shown near the Bragg peak (a) and in a wider spectral interval (b) of the optical systems consisting of the multilayer mirror M5 combined with a $MoSi_2/Si_3N_4$ (500/50 nm) (*curve 2*) free-standing absorbing filter. *Curve 1* is the target reflectivity. The vertical dashed lines indicate the optimization interval.

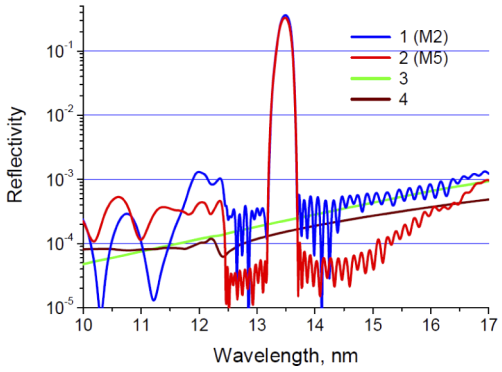


**Fig. 8.** Reflectivity (in absolute units) versus the wavelength of the mimic mirrors M2 (*curve 1*) and M5 (*curve 2*) as well as of a single $MoSi_2$-Si interface (*curve 3*) and of an uncoated fused silica substrate (*curve 4*).

As stated at the end of section 2, for all examples of optimized mimic mirrors, we have used as the starting point of the optimization a periodic $MoSi_2$/Si mirror with a number of bi-layers $N = 100.5$, as this number seems quite practicable from a technological point of view. However, one can ask how the performance of the mimic mirrors would be impacted with a different number of bi-layers. Decreasing the number of bi-layers down to, for instance, $N = 75.5$ would essentially result in a degradation of all fidelity parameters, with their values increasing by a factor of about 3 at $\rho_{max} = 3 \cdot 10^{-4}$. On the other hand, increasing the number of bi-layers up to, for instance, $N = 125.5$ would result in a modest decrease of the parameters $\chi_1$ and $\chi_3$ ($\sim 20\%$ at $\rho_{max} = 3 \cdot 10^{-4}$), while keeping the same value of the parameter $\chi_2$. Further increasing the number of bi-layers would result in additional decrease of the fidelity parameters, but it would also result in a higher likelihood of technological inaccuracies during the fabrication of the mimic mirror. As a trade-off between the two trends, and to illustrate our approach and its basic properties, we consider the example of $N = 100.5$ bilayers as typical number for the present case study. Ultimately, the optimum choice of the bi-layers number can be only made on the basis of the experimental data analysis, and depending on the specific spectrum that is to be mimicked.

Optics EXPRESS

## 4. Mimic mirrors for use in dual reflection

Mimicking target spectra with a single reflection, such as with M4 or M5 is a means for high-fidelity characterization of the in-band power of EUV sources in lithography systems [22]. However, a more specific comparison of sources can be done in terms of their brightness, which specifies the power within the targeted in-band spectrum also per source area and emission solid angle. For this task, spectrally selective mirror telescopes have been employed based on two narrowband mimic mirrors operating near normal incidence with the goal of imaging only the in-band spectral component on a spatially resolving detector [14,15]. However, there the spectrum selected by the two imaging mirrors did not match the target spectrum. Therefore, additional spectral recordings of the in-band and out-of-band radiation became required with a set of calibrated spectrometers [23].

In order to facilitate according brightness measurements, we investigate in the following the option for designing multilayer mirrors that mimic the target spectrum after two subsequent reflections. As described above, to simplify the optimization procedure, we begin with choosing an appropriate absorber material. The $MoSi_2$/Si multilayer structures presented above for use in single reflection are less suited here, because their spectral bandpass after two reflections becomes narrower than the width of the target spectrum. To obtain a broader spectral width it is most convenient to choose an absorber material that offers a higher polarizability than $MoSi_2$.

In the following, we consider $Ru_2Si_3$/Si multilayer mirrors only to illustrate a possible design, since we do not know if fabricating multilayer structures containing $Ru_2Si_3$ has already been attempted. Nevertheless, such choice of absorber materials is promising because $Ru_2Si_3$-Si interfaces are expected to be stable, similar to $MoSi_2$-Si, while the polarizability of $Ru_2Si_3$ at 13.5 nm wavelength exceeds that of $MoSi_2$ by a factor of about 1.5. As a starting point for the optimization algorithm we consider an initial, periodic $Ru_2Si_3$/Si multilayer stack with layer thicknesses of 2.34 and 4.75 nm for $Ru_2Si_3$ and Si, respectively, comprising again 100.5 bi-layers. The calculated reflectivity curve after two-fold reflection from the periodic $Ru_2Si_3$/Si multilayer mirror is shown in Fig. 9 as curve 2, and one can see that the spectral width of two-fold reflection coincides well with the target curve.

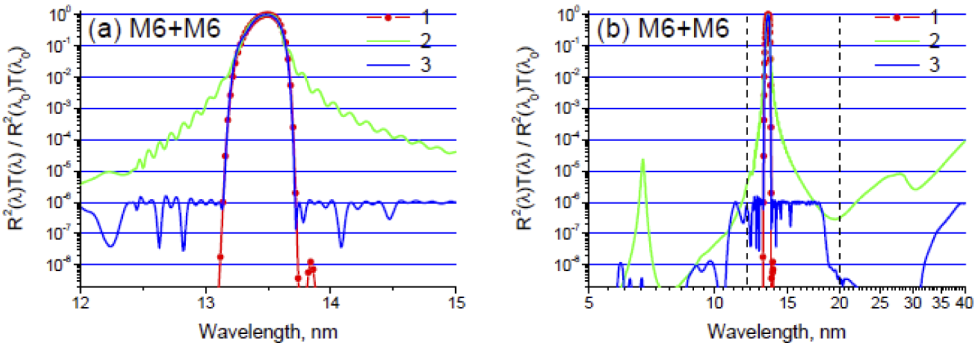


**Fig. 9.** *Curve 3*: Total transmittance versus wavelength shown near the Bragg peak (a) and in a wider spectral interval (b) of the optical systems consisting of two multilayer mirrors M6 ($Ru_2Si_3$/Si) combined with a $MoSi_2/Si_3N_4$ (300/50 nm) free-standing absorbing filter. *Curve 2* is the reflectivity from two periodic $Ru_2Si_3$/Si multilayers used as the initial starting point for the optimization. *Curve 1* is the target reflectivity. The vertical dashed lines indicate the optimization interval.

For calculating optimized designs with aperiodic multilayer stacks, the multilayer reflectivity $R(\lambda)$ in Eq. (2) was replaced by $R^2(\lambda)$ to ensure that the target reflectivity, $R_0$, is now approached with dual reflection at two equal mimic mirrors. During the optimization of the multilayer

Optics EXPRESS

structure we lowered the maximum out-of-band reflectivity significantly, down to a value of $1 \cdot 10^{-6}$. To suppress a parasitic peak at about 40 nm wavelength, we increased the thickness of the $MoSi_2$ layer in the transmission filter to 300 nm. The resulting depth-distribution of the layer thicknesses of the mimic $Ru_2Si_3$/Si mirror, named M6, is shown in Fig. 2. The calculated reflectivity curve after two-fold reflection, taking into account the transmittance of the free-standing $MoSi_2/Si_3N_4$ (300/50 nm) filter, is shown in Fig. 9 as curve 3. One can see that dual reflection from M6 mimics the shape and bandwidth of the target Bragg peak very well, and that out-of-band radiation is very strongly suppressed. The according fidelity parameter $\chi_1$ is extremely small (see Table 1), indicating that the spectrally integrated out-of-band radiation with regard to the overall transmission amounts to only 0.0037%.

## 5. Multilayer mirrors with reduced variation of the layer thickness

The reflectivity spectra presented so far indicate a significant potential for designing optimized mimic mirrors, however, it is required to consider feasibility of fabrication as well. Specifically, Fig. 2 shows that there can be considerable variations in the thickness of $MoSi_2$, $Ru_2Si_3$/Si and Si layers, particularly at the top and bottom of the layer stack. Such variations can be problematic in fabrication because, for instance, the material density of a thin film may vary with thickness and lead to uncertainties in the fabricated dielectric constant. As an example, with Mo one observes a transition from amorphous to crystalline growth at a thickness of about 2 to 2.2 nm [24]. To minimize such fabrication uncertainties, the question arises whether it is possible to reduce the variation in layer thickness from layer-to-layer of an aperiodic mimic mirror without much degrading its optical properties.

To investigate this question, we extend our previous merit function, $MF$ in Eq. (3), to a total merit function, $MF_1$, with an extra term [18,25] that enables optimization of aperiodic multilayers also towards smaller variation in the layer thickness:

$$MF_1 = MF + \frac{Q_S}{d_{min}^2} \sum_j \left[ \left(d_{2j+1} - d_{2j-1}\right)^2 + \left(d_{2j+2} - d_{2j}\right)^2 \right] \tag{4}$$

In this expression, $Q_S$ is an additional optimization parameter which controls minimization of the difference in thicknesses of all odd (Si) and even ($MoSi_2$) layers. The constant $d_{min} = 1$ nm is introduced in order to keep the parameter $Q_S$ dimensionless. If $Q_S = 0$, we obtain the conventional merit function as in Eq. (3). If $Q_S$ tends to infinity, the minimization of Eq. (4) will result in a periodic multilayer structure.

Using the merit function in Eq. (4) with the periodic $MoSi_2$/Si multilayer as an initial design and setting the parameters $Q_S$ to $3 \cdot 10^{-4}$ and $\rho_{max}$ to $1 \cdot 10^{-3}$, we obtain the mirror M7, whose layer thickness distribution is shown in Fig. 10. For the optimization, a $MoSi_2/Si_3N_4$ (250/50 nm) absorbing filter was taken into account, i.e., the mirror M7 is analogous to the mirror M2 considered before. The total transmittance of the mimic optical system M7 is shown in Fig. 11 as curve 2. Comparing the layer thickness distributions of M7 (Fig. 10) and M2 (Fig. 2) demonstrates that the distribution of M7 is much smoother than that of M2, while the fidelity parameters $\chi_1$ and $\chi_3$ (see Table 1) are almost the same. The parameter $\chi_2$ for M7, specifying the spectral shape fidelity of the Bragg peak, did increase by a factor of two as compared with M2, however its value its value is still small, at the level of only a few percent shape deviation.

The mirror M8 was designed with the same parameters $Q_S = 3 \cdot 10^{-4}$ and $\rho_{max} = 1 \cdot 10^{-3}$ and the same absorbing filter as M7, but the initial design was mirror M2. The depth-distribution of layer thickness for M8 is shown in Fig. 10, and as can be seen, it is also smoother than that of M2, while the fidelity parameters remain close to those of mirror M7. The total transmittance of the mimic optical system M8 is shown in Fig. 11 as curve 3.

From a larger set of according optimization calculations we observe that it is possible to design multilayers with even smoother distribution of the layer thickness than that of M7 and M8 by

Optics EXPRESS

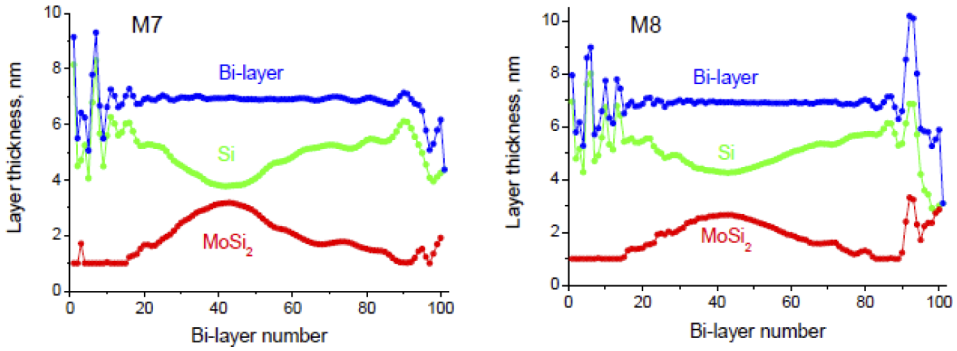


**Fig. 10.** Depth-distributions of layer thickness for the mimic multilayer mirrors M7 and M8, with a reduced variation of the layer thickness. The bi-layer number is counted from the top of the mirror. The natural oxide layer taken into account in the calculations is not shown in these graphs.

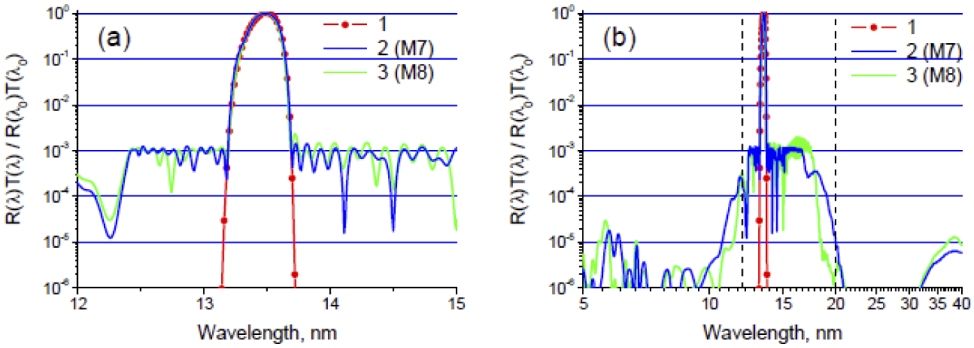


**Fig. 11.** Total transmittance versus wavelength shown near the Bragg peak (a) and in a wider spectral interval (b) of the optical systems consisting of the multilayer mirror M7 (*curve 2*) or M8 (*curve 3*) with a reduced variation of the layer thickness, combined with a $MoSi_2/Si_3N_4$ (250/50 nm) free-standing absorbing filter. *Curve 1* is the target reflectivity. The vertical dashed lines indicate the optimization interval.

further increasing the parameter $Q_S$, but that this also increases all fidelity parameters. The optimal choice for a design to be fabricated should thus be selected as a compromise between the specific optical target parameters for the required application and the available fabrication technology for the selected material combination.

## 6. Conclusions

We presented a general method for designing mimic XUV optical systems able to reproduce the spectral reflectivity peak of a given transmission spectrum by combining aperiodic multilayers and free-standing absorbing layers. We showed how to choose an initial design based on a periodic multilayer mirror and how to optimize this design in order to achieve the desired transmission spectrum. The optimization process is based on the minimization of a merit function and the degree of agreement with the target spectrum is quantified through the use of three fidelity parameters. Additional optimization allows to reduce layer-to-layer thickness variations, resulting in aperiodic mirrors with a smoother layer thickness distribution, making the design more suitable for fabrication. For specificity in demonstrating the approach for optimization, we have shown the design of a mimic optical system reproducing the reflectivity peak at 13.5

Optics EXPRESS

nm of 12 subsequent, identical Mo/Si multilayer mirrors. The resulting mimic mirrors, M2 to M8, show a high fidelity in reproducing the target spectrum and thus, a high potential of application for metrology of EUV sources. Because our approach is of general applicability, the same optimization process can be used to mimic the throughput of any XUV optical system with a narrowband and smooth (single-peaked) spectrum. The next step towards the demonstration and the efficiency of our optimization process would be the actual fabrication and qualification of such mimic optical systems.

## A. Appendix: Discussion on the influence of fabrication-related errors

In the following we discuss the influence of deviations from the approximations that were used to calculate optimized multilayer mirrors. However, due to the high number of the involved multilayer parameters, i.e., hundreds of geometrical and optical specifications describing the individual layers, and also many global parameters, such as surface roughness, wavefront curvature and layer intermixing, a complete survey is impossible to give. To give nevertheless a broader overview, we investigate the influence of the most important effects on the fidelity parameters, in the form of examples with typical numbers. A summary of the expected strength of the effects is given in Table 2 for the two best-performing mimic mirrors, M5 and M7. M7 is characterized by the smoothest layer thickness depth distribution and thus appears to be most suitable for fabrication with high fidelity. M5 provides the smallest value of the fidelity parameter $\chi_1$, while its layer thickness distribution at the top and bottom oscillates quite strongly.

**Table 2. Effect of various deviations due to fabrication on the fidelity parameters of the mirrors M7 and M5.**

| Factors influencing the fidelity parameters | | Mirror M7 + filter | | | Mirror M5 + filter | | |
|---|---|---|---|---|---|---|---|
| | | $\chi_1$ | $\chi_2$ | $\chi_3$ | $\chi_1$ | $\chi_2$ | $\chi_3$ |
| 1 Ideal mirror | | $1.9 \cdot 10^{-2}$ | $5.8 \cdot 10^{-2}$ | $1.4 \cdot 10^{-3}$ | $1.8 \cdot 10^{-3}$ | $5.7 \cdot 10^{-2}$ | $2.9 \cdot 10^{-4}$ |
| 2 Material density: $\rho = 0.95\rho_{bulk}$ | | $1.8 \cdot 10^{-2}$ | $6.3 \cdot 10^{-2}$ | $1.5 \cdot 10^{-3}$ | $1.9 \cdot 10^{-3}$ | $4.8 \cdot 10^{-2}$ | $2.5 \cdot 10^{-4}$ |
| 3 Absorptivity: $\mathrm{Im}(\varepsilon_{Si}) = 1.2\mathrm{Im}(\varepsilon_{ideal})$ | | $2.0 \cdot 10^{-2}$ | $6.0 \cdot 10^{-2}$ | $1.5 \cdot 10^{-3}$ | $2.1 \cdot 10^{-3}$ | $7.1 \cdot 10^{-2}$ | $3.1 \cdot 10^{-4}$ |
| 4 Interfacial roughness: $\sigma = 0.3$ nm | | $1.9 \cdot 10^{-2}$ | $7.0 \cdot 10^{-2}$ | $1.6 \cdot 10^{-3}$ | $1.8 \cdot 10^{-3}$ | $6.1 \cdot 10^{-2}$ | $3.5 \cdot 10^{-4}$ |
| 5 $SiO_2$ layer thickness: $d = 2.5$ nm | | $2.5 \cdot 10^{-2}$ | $4.8 \cdot 10^{-2}$ | $2.1 \cdot 10^{-3}$ | $4.6 \cdot 10^{-3}$ | $6.1 \cdot 10^{-2}$ | $5.3 \cdot 10^{-4}$ |
| 6 Bi-layers thickness: $d = 1.01d_{ideal}$, $\varphi = 12.65°$ | | $1.9 \cdot 10^{-2}$ | $5.4 \cdot 10^{-2}$ | $1.7 \cdot 10^{-3}$ | $1.8 \cdot 10^{-3}$ | $3.9 \cdot 10^{-2}$ | $3.8 \cdot 10^{-4}$ |
| 7 Si layers thickness: $d = 1.01d_{ideal}$, $\varphi = 11.88°$ | | $2.1 \cdot 10^{-2}$ | $3.9 \cdot 10^{-2}$ | $1.0 \cdot 10^{-2}$ | $2.9 \cdot 10^{-3}$ | $3.3 \cdot 10^{-2}$ | $4.2 \cdot 10^{-3}$ |
| 8 $MoSi_2$ layers thickness: $d = 1.01d_{ideal}$, $\varphi = 10.92°$ | | $2.0 \cdot 10^{-2}$ | $9.1 \cdot 10^{-2}$ | $4.0 \cdot 10^{-3}$ | $2.5 \cdot 10^{-3}$ | $9.2 \cdot 10^{-2}$ | $1.8 \cdot 10^{-3}$ |
| 9 Random layer fluctuations | $\Delta d = 0.03$ nm | $2.1 \cdot 10^{-2}$ | $9.9 \cdot 10^{-2}$ | $5.2 \cdot 10^{-3}$ | $3.6 \cdot 10^{-3}$ | $1.0 \cdot 10^{-1}$ | $2.5 \cdot 10^{-3}$ |
| | $\Delta d = 0.045$ nm | $2.4 \cdot 10^{-2}$ | $1.4 \cdot 10^{-1}$ | $9.2 \cdot 10^{-3}$ | $6.1 \cdot 10^{-3}$ | $1.5 \cdot 10^{-1}$ | $5.6 \cdot 10^{-3}$ |
| | $\Delta d = 0.06$ nm | $2.8 \cdot 10^{-2}$ | $1.7 \cdot 10^{-2}$ | $1.4 \cdot 10^{-2}$ | $9.4 \cdot 10^{-3}$ | $2.1 \cdot 10^{-1}$ | $9.1 \cdot 10^{-3}$ |

### *A.1. Influence of wavefront curvature*

For the optimization of layer thickness distributions for mimic mirrors we made use of the plane wave approximation by assuming that the angle of incidence is the same across the entire mirror surface. In the case of an XUV source, this assumption is approximately justified because the size of the source is typically small (for instance a few hundred micrometers) while the first mirror is at a relatively large distance. Considering an approximately spherical wave front arriving at a plane mirror, the angle of incidence across the mirror surface varies in the interval $[\varphi - \Delta\varphi, \varphi + \Delta\varphi]$, where $\varphi$ is the average angle of incidence and where $\Delta\varphi = D/(2L)$, with $L$ the distance from source to mirror and D the mirror diameter. If we take a typical distance from the source $L = 1$ m, then $D = 5$ mm as the standard diameter of a free-standing $Si_3N_4$ substrate used as the absorbing filter in front of the mimic mirror [12], and an angle of incidence $\varphi = 10°$, we

Optics EXPRESS

obtain $\Delta\varphi = 2.5 \cdot 10^{-3}$ rad. The according spectral widening of the Bragg peak at $\lambda = 13.5$ nm then amounts to a small value of $\Delta\lambda \approx 2\Delta\varphi \cdot \lambda \cdot \tan(\varphi) \approx 0.012$ nm, which can be neglected in practice.

### A.2. Influence of deviating optical material constants

When optimizing a multilayer mirror via the layer thicknesses, it is assumed that the optical constants of the involved materials are known. However, this assumption does not account for inaccuracies in optical constants of optical data bases [20], deviations of the density of materials as fabricated from those used in calculations, or the presence of admixtures (e.g., oxygen and argon in magnetron sputtering) introduced during a mirror deposition. As an example, row 2 in Table 2 shows the fidelity parameters for the case where the density of both materials is 0.95 of the bulk density. Similarly, row 3 shows the effect of increasing the absorptivity of the Si layers by 20%. For comparison, row 1 shows the fidelity parameters in the case of an ideal mirror optimization. It can be seen that both types of deviation do not change the fidelity parameters much for both investigated mirrors. From this we conclude that the effect of small inaccuracies in optical constant is negligible in practice.

### A.3. Influence of interfacial roughness

Row 4 in Table 2 gives an example of the effect of interfacial roughness on the fidelity parameters. As a typical value we assumed a rms height roughness of 0.3 nm. Accounting for surface roughness was achieved via the Nevot-Croce factor for the amplitude reflectance from each interface. It can be seen that the assumed surface roughness has little effect on the fidelity parameters.

### A.4. Influence of top surface oxidation layer

In the calculations we assumed that there is a natural oxide layer on top of the multilayer stack with a typical thickness of 1.5 nm. However, the oxidized layer thickness in known to increase with time when exposed to hard radiation load [26]. For instance, if the oxidized layer thickness increases by 1 nm, the thickness of the uppermost Si layer decreases accordingly, by about 0.46 nm. For such numbers, row 5 in Table 2 shows that for M5 the parameter $\chi_1$ is increased by a factor of 2.5, and further increase is expected with progressing oxidation. To suppress oxidation, a cap layer can be placed on the mirror top, such as is done with mirrors used in EUVL optical systems. However, as the present work aims only to present the general options for designing mimic mirrors, we did not pursue optimization with specific cap layers.

### A.5. Influence of systematic bi-layer thickness deviation

In multilayer fabrication, a systematic (deterministic) deviation of layer thicknesses from the desired values can occur, for instance via a variation in the flux of particles due to an erosion of the magnetron target. As a first example we consider that the thickness of all layers ($MoSi_2$ and Si) is increased by 1%. Consequently, following the Bragg law, the reflectivity peak is shifted by $\Delta\lambda/\lambda \approx \Delta d/d \cdot \cot(\varphi)$, where $\varphi$ is the incidence angle, i.e., the Bragg peak shifts by $\Delta\lambda \approx 0.14$ nm. This shift is relatively large; however, it can also be compensated quite easily with a mirror alignment, namely, via increasing the incident angle by 2.65° to a value of 12.65° as assumed for the data in row 6 of Table 2. After such alignment, the spectral dependence of the mimic mirror reflectance as well as the fidelity parameters remain practically the same as for the ideal mirror.

As a second type of systematic deviation we consider that the thickness of the $MoSi_2$ layers corresponds to the ideal structure, while the thickness of the Si layers is increased by 1%. As displayed in row 7 of Table 2, we also observe in this case that increasing the incident angle (by 1.88° to a value of 11.88°) can compensate for the shift of the Bragg peak, while keeping the

Optics EXPRESS

parameters $\chi_1$ and $\chi_2$ almost unchanged. The parameter $\chi_3$ is noticeably increased by a factor of about 7 or 14.5, for mirror M7 or M5, respectively.

For a closer analysis of this increase of the parameter $\chi_3$, Fig. 12 displays the transmittance of the system consisting of the mimic mirror M7 and the absorbing filter, where curve 2 corresponds to the ideal mirror and curve 3 to the mirror with 1% increase in the thickness of all Si layers. It can be seen in Fig. 12(a) that the increase of the parameter $\chi_3$ is caused by a narrow peak arising in the immediate vicinity of the main Bragg peak. The parasitic peak is so narrow that it is not clearly visible in Fig. 12(b), but rather shows as a small deformation of the main peak. Taking into account that the parameter $\chi_1$ is practically unchanged, we conclude that a 1% systematic deviation of the Si layers thickness can be considered as tolerable for most applications.

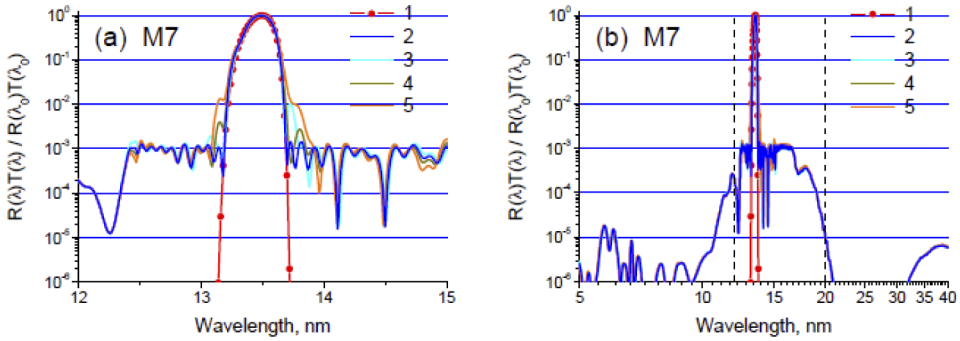


**Fig. 12.** Total transmittance versus wavelength shown near the Bragg peak (a) and in a wider spectral interval (b) of the optical system consisting of mirror M7 and a free-standing absorbing filter. *Curve 2* was calculated assuming an ideal mirror. *Curve 3* was calculated assuming that the thickness of all Si layers is increased by 1%. *Curves 4* and *5* were calculated assuming that the thickness of all MoSi2 layers is increased by 1% and 2.5%, respectively. For compensating for the shift of the Bragg peak, the angles of incidence are set to 10° (*2*), 11.88° (*3*), 10.92° (*4*) and 12.1° (*5*). *Curve 1* is the target reflectivity. The vertical dashed lines indicate the optimization interval.

For another type of systematic deviation, we consider the opposite of the previous example and set now the thickness of all Si layers to correspond to the ideal structure, while the thickness of all $MoSi_2$ layers is increased by 1%. The corresponding spectrum is displayed in Fig. 12 as curve 4 and the fidelity parameters are in row 8 of Table 2. In this case, the parameter $\chi_1$ is unchanged, while the parameter $\chi_3$ is increased by a factor of 3 or 6, for mirror M7 or M5, respectively. Here also, we can conclude that a 1% systematic deviation of the MoSi2 layers thickness can be considered practicable.

However, while a 1% variation in Si layers thickness corresponds to about 0.05 nm, limiting the $MoSi_2$ layers to the same deviation requires a layer thickness control as low as 0.02 nm. If such precise control is not possible and the $MoSi_2$ layers thickness would deviate more strongly, e.g., by 2.5% (i.e., by 0.05 nm in average), then the deformation of the main peak would become more pronounced (see curve 5 in Fig. 12), increasing the parameter $\chi_3$ to about 0.02 for both mirrors. We conclude that a deviation in $MoSi_2$ layers thickness can be a factor that noticeably limits the performance of the mimic mirrors, if the deviation is larger than about 20 to 50 pm. The deposition of layers with such accuracy is clearly a difficult challenge, however, according accuracies can be reached with state-of-the-art deposition technology. For instance, in experimental investigations of short-period W/Si mirrors with up to 400 bi-layers of 2.5 nm thickness [27], a maximum systematic deviation of the bi-layer thickness smaller than 13 pm was realized throughout the entire layer stack.

Optics EXPRESS

### A.6. Influence of bi-layer thickness stochastic errors

The systematic deviations in multilayer mirrors discussed so far can be considered deterministic. This means that, after additional experimental analysis of the internal structure of multilayer mirrors, one can take them into account when designing a mimic mirror. However, stochastic imperfections of multilayer structures, such as due to random fluctuations of the incident particle flux during layer growth, cannot be included in the optimization procedure. To estimate the effect of such unpredictable deviations, we analyze below the effect of random layer fluctuations on the mimic mirror performance.

For conveniently quantifying the strength of the random deviations, we assume that the layer thickness is evenly distributed within a certain, small interval of width $\pm\Delta d$ around the average thickness $d$. Reflectivity calculations are performed for three different strengths of deviations, according to $\Delta d = 0.03$, 0.045, and 0.06 nm, and for $10^3$ different realizations (sets) of mirror layer thickness. For each deviation interval we calculate the probability density function $p(\chi)$ of the fidelity parameters $\chi$ normalized with $\int p(\chi)\mathrm{d}\chi = 1$. The results are shown in Fig. 13, where the vertical dashed lines indicate the parameter value obtained with the ideal mimic systems comprising of mirrors M7 and M5 with absorbing filters. To quantify the maximum fidelity parameter represented by its distributions, we take the value $\tilde{\chi}$ of the fidelity parameters such that 75% of the distribution area is included, i.e., $\int_0^{\tilde{\chi}} p(\chi)\mathrm{d}\chi = 0.75$. This choice corresponds to the situation where, in average, three out of four fabricated mirrors would show a fidelity parameter smaller than $\tilde{\chi}$. The according maximum fidelity parameters are presented in Table 2, row 9.

First, inspecting the influence of layer deviations on mirror M7, it can be seen that the most important fidelity parameter, $\chi_1$, is not much affected. For instance, if setting $\Delta d$ to a value of 0.03 or 0.045 nm, the parameter $\chi_1$ remains below 0.021 or 0.024, respectively. Such values are quite comparable to what is obtained in the absence of deviations (0.019 for the ideal mirror M7). For the mirror M5, the corresponding fidelity values are 0.0036 or 0.0061, i.e., they are increased by a factor of 2 or 3.4 compared to the ideal mirror M5. Nonetheless, the absolute values of $\chi_1$ for M5 still remain much lower than even those of even an ideal mirror M7.

Turning to the second fidelity parameter, $\chi_2$, as shown in Fig. 13, its distribution is almost the same for both mirrors M7 and M5. The values found are moderate factors, between two and four, as compared to those for the respective ideal mirrors. As an example, the largest value found is $\chi_2 = 0.32$, obtained for the mirror M7 mirror with $\Delta d = 0.045$ nm. In this case $\chi_1$ remains small ($\chi_1 = 2.9 \cdot 10^{-2}$), however, $\chi_3$ increases noticeably ($\chi_3 = 3.5 \cdot 10^{-2}$). On the other hand, if the angle of incidence is slightly increased to 10.65° (such as via slight realignment in an experiment), then the values of all fidelity parameters improve again, decreasing to $\chi_1 = 2.6 \cdot 10^{-2}$, $\chi_2 = 0.11$ and $\chi_3 = 1.4 \cdot 10^{-2}$.

An interesting observation can be made in Figs. 13(c) and 13(d). Unexpected on a first view, one can see that introducing random layer deviations may even result in a decreased fidelity parameter $\chi_2$ as compared to an ideal mirror. However, such improvement of a single fidelity parameter is in fact is not too surprising when remembering that the designs of the ideal mirrors are obtained via minimizing all three fidelity parameters simultaneously. Correspondingly, the improvement of a single parameter should then be accompanied by the increase of another fidelity parameter. Indeed, for instance, we find that randomizing the layers of M7 with $\Delta d = 0.03$ nm, improves $\chi_2$ ($\chi_2 = 4.3 \cdot 10^{-2}$) beyond that of the ideal mirror. However, at the same time, $\chi_3$ is increased to a value of $6.3 \cdot 10^{-3}$ (i.e. by a factor of 4.5 compared to the ideal mirror). The randomization leaves the parameter $\chi_1$ almost unchanged ($\chi_1 = 2.1 \cdot 10^{-2}$).

Turning to the third fidelity parameter, $\chi_3$ essentially increases for both mirrors when compared to the ideal case, for instance by a factor $\sim 10$ and $\sim 30$ for mirror M7 and M5, respectively, for the largest deviation considered ($\Delta d = 0.06$ nm). As is reported above, this is usually due to a single, very narrow peak in the immediate vicinity of the main Bragg peak, which often can be neglected in practice.

Optics EXPRESS

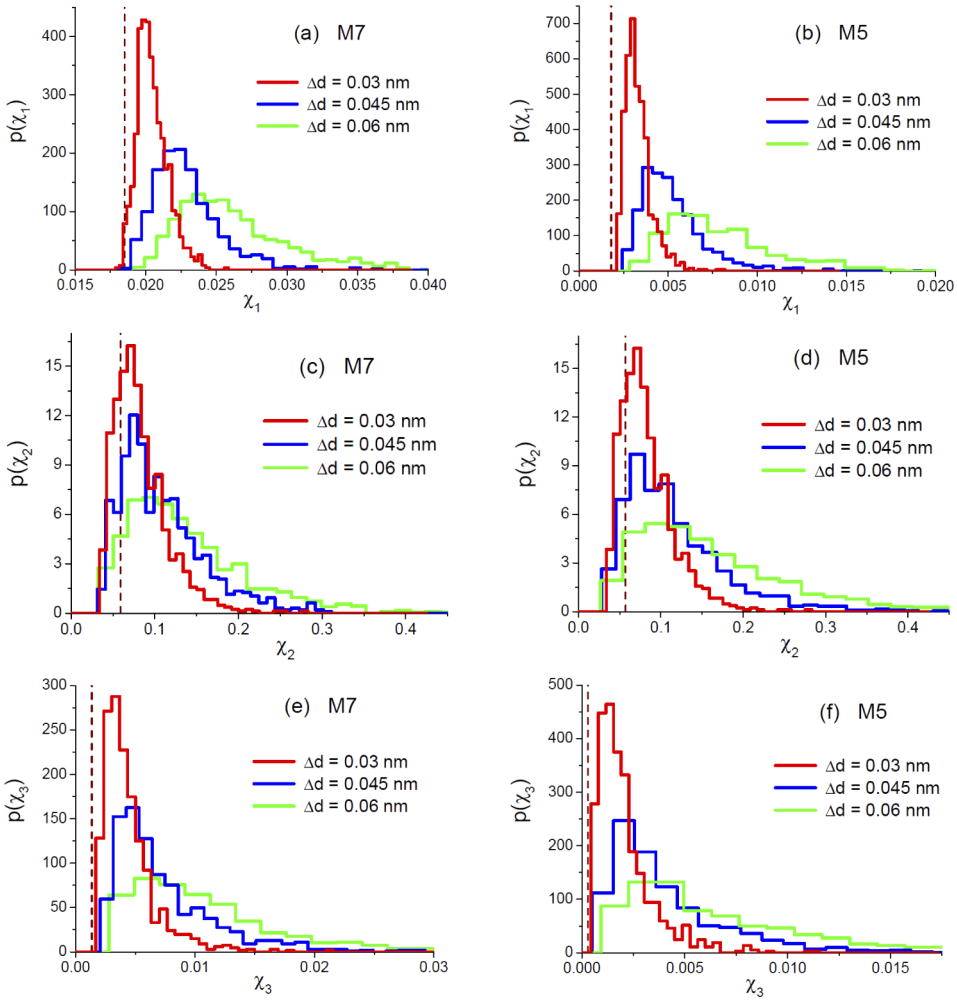


**Fig. 13.** Probability density function $p(\chi)$ of the parameters $\chi$ distribution due to random fluctuations of layers thickness in M7 and M5 mimic mirrors. Fluctuations were assumed to be evenly distributed in the $\pm\Delta d$ interval, where $\Delta d$ = 0.03, 0.045, or 0.06 nm. Vertical dashed lines indicate the value of parameters $\chi$ for ideal mirrors without layer fluctuations.

In summary, the mirror M7 is expected to be relatively insensitive with respect to random thickness deviations during fabrication as compared to mirror M5. In particular, the fidelity parameter $\chi_1$ of M7 is almost unchanged even with rather large deviations ($\Delta d$ = 0.06 nm), while for M5, $\chi_1$ increases by a factor between 2 and 5. The absolute values of the parameters $\chi_1$ and $\chi_3$ remain considerably lower for the mirror M5. In particular, the value of the most important fidelity parameter, $\chi_1$, for the mirror M5 remains lower than for the ideal mirror M7, even for $\Delta d$ = 0.06 nm.

A final note on the discussion of deviations in mirror fabrication is that the considerations are solely meant to give an overall indication of the expected relative strengths of different effects and are by no means complete. For instance, even with the same random fluctuations of deposition flux, one would likely obtain differently sized layer deviations when growing the layer stack for M5 vs growing M7, simply because the targeted layer distributions are different in this case, more oscillating (M5) or smoother (M7). Therefore, choosing between M7 and M5 mirrors should

Optics EXPRESS

currently be based on a direct experimental comparison and be investigated with regard to the specific mimicking task to be performed.

## Funding

Ministry of Education and Science of the Russian Federation; NanoNextNL.

## Acknowledgments

The authors thank Ani Chandrasekaran, from the XUV Optics group at the University of Twente (Enschede, The Netherlands) for providing the experimental EUV reflectivity spectra used in this work.

## References

1. C. Wagner and N. Harned, "EUV lithography: Lithography gets extreme," Nat. Photonics **4**(1), 24–26 (2010).
2. J. Ojeda, C. A. Arrell, J. Grilj, F. Frassetto, L. Mewes, H. Zhang, F. van Mourik, L. Poletto, and M. Chergui, "Harmonium: A pulse preserving source of monochromatic extreme ultraviolet (30–110 eV) radiation for ultrafast photoelectron spectroscopy of liquids," Struct. Dyn. **3**(2), 023602 (2016).
3. A. Torrisi, P. Wachulak, Ł. Węgrzyński, T. Fok, A. Bartnik, T. Parkman, Š. Vondrová, J. Turňová, B. J. Jankiewicz, B. Bartosewicz, and H. Fiedorowicz, "A stand-alone compact EUV microscope based on gas-puff target source," J. Microsc. **265**(2), 251–260 (2017).
4. F. Barkusky, A. Bayer, S. Döring, B. Flöter, P. Grossmann, C. Peth, M. Reese, and K. Mann, "Applications of compact laser-driven EUV/XUV plasma sources," Proc. SPIE **7361**, 736112 (2009).
5. N. R. Boewering, J. R. Hoffman, O. V. Khodykin, C. L. Rettig, B. A. M. Hansson, A. I. Ershov, and I. V. Fomenkov, "Metrology of laser-produced plasma light source for EUV lithography," Proc. SPIE **5752**, 1248–1256 (2005).
6. M. S. Bibishkin, N. I. Chkhalo, S. A. Gusev, E. B. Kluenkov, A. Y. Lopatin, V. I. Luchin, A. E. Pestov, N. N. Salashchenko, L. A. Shmaenok, N. N. Tsybin, and S. Y. Zuev, "Multilayer Zr/Si filters for EUV lithography and for radiation source metrology," Proc. SPIE **7025**, 702502 (2008).
7. N. I. Chkhalo, M. N. Drozdov, E. B. Kluenkov, A. Y. Lopatin, V. I. Luchin, N. N. Salashchenko, N. N. Tsybin, L. A. Sjmaenok, V. E. Banine, and A. M. Yakunin, "Free-standing spectral purity filters for extreme ultraviolet lithography," J. Micro/Nanolith. MEMS MOEMS **11**(2), 021115 (2012).
8. V. V. Medvedev, A. J. R. van den Boogaard, R. van der Meer, A. E. Yakshin, E. Louis, V. M. Krivtsun, and F. Bijkerk, "Infrared diffractive filtering for extreme ultraviolet multilayer Bragg reflectors," Opt. Express **21**(14), 16964–16974 (2013).
9. Q. Huang, M. de Boer, J. L. P. Barreaux, R. van der Meer, E. Louis, and F. Bijkerk, "High efficiency structured EUV multilayer mirror for spectral filtering of long wavelengths," Opt. Express **22**(16), 19365–19374 (2014).
10. Q. Huang, D. M. Paardekooper, E. Zoethout, V. V. Medvedev, R. van de Kruijs, J. Bosgra, E. Louis, and F. Bijkerk, "UV spectral filtering by surface structured multilayer mirrors," Opt. Express **39**(5), 1185–1188 (2014).
11. N. I. Chkhalo, M. N. Drozdov, E. B. Kluenkov, S. V. Kuzin, A. Y. Lopatin, V. I. Luchin, N. N. Salashchenko, N. N. Tsybin, and S. Y. Zuev, "Thin film multilayer filters for solar EUV telescopes," Appl. Opt. **55**(17), 4683–4690 (2016).
12. J. L. P. Barreaux, I. V. Kozhevnikov, M. Bayraktar, R. W. E. van de Kruijs, H. M. J. Bastiaens, F. Bijkerk, and K.-J. Boller, "Narrowband and tunable anomalous transmission filters for spectral monitoring in the extreme ultraviolet wavelength region," Opt. Express **25**(3), 1993–2008 (2017).
13. M. Lowisch, P. Kuerz, H. J. Mann, O. Natt, and B. Thuering, "Optics for EUV production," Proc. SPIE **7636**, 763603 (2010).
14. F. Bijkerk, S. Alonso van der Westen, C. C. de Bruijn, A. E. Yakshin, R. Stuik, C. Bruineman, and V. Bakshi, "FC2 project status & metrology survey," *International Sematech EUV Source Workshop*, Santa Clara, California (2003).
15. S. Alonso van der Westen, C. Bruineman, E. Louis, C. C. de Bruijn, F. Bijkerk, S. Grantham, M. W. McGeoch, and V. Bakshi, "Flying Circus 2 status and update," *International Sematech EUV Source Workshop*, Santa Clara, California (2004).
16. A. A. Zameshin, A. E. Yakshin, A. Chandrasekaran, and F. Bijkerk, "Angular and spectral bandwidth of extreme UV multilayers near spacer material absorption edges," J. Nanosci. Nanotechnol. **19**(1), 602–608 (2019).
17. I. V. Kozhevnikov, I. N. Bukreeva, and E. Ziegler, "Design of X-ray supermirrors," Nucl. Instrum. Methods Phys. Res., Sect. A **460**(2-3), 424–443 (2001).
18. I. V. Kozhevnikov, A. E. Yakshin, and F. Bijkerk, "Wideband multilayer mirrors with minimal layer thicknesses variation," Opt. Express **23**(7), 9276–9283 (2015).
19. V. V. Kondratenko, Y. P. Pershin, O. V. Poltseva, A. I. Fedorenko, E. N. Zubarev, S. A. Yulin, I. V. Kozhevnikov, S. I. Sagitov, V. A. Chirkov, V. E. Levashov, and A. V. Vinogradov, "Thermal stability of soft x-ray Mo-Si and $MoSi_2$-Si multilayer mirrors," Appl. Opt. **32**(10), 1811–1816 (1993).
20. CXRO X-Ray Database, "*X-Ray Interactions With Matter*," (The Center for X-Ray Optics, 2010), http://henke.lbl.gov/optical_constants/.

Optics EXPRESS


21. J. E. Dennis Jr. and R. B. Schnabel, *Numerical methods for unconstrained optimization and nonlinear equations* (Prentice-Hall, Englewood Cliffs, NJ, 1983).
22. T. Missalla, M. C. Schuermann, R. Lebert, C. Wies, L. Juschkin, R. M. Klein, F. Scholze, G. Ulm, A. Egbert, B. Tkachenko, and B. N. Chichkov, "Metrology tools for EUV-source characterization and optimization," Proc. SPIE **5374**, 979–990 (2004).
23. H. Komori, Y. Ueno, H. Hoshino, T. Ariga, G. Soumagne, A. Endo, and H. Mizoguchi, "EUV radiation characteristics of a $CO_2$ laser produced Xe plasma," Appl. Phys. B **83**(2), 213–218 (2006).
24. S. Bajt, D. G. Stearns, and P. A. Kearney, "Investigation of the amorphous-to-crystalline transition in Mo/Si multilayers," J. Appl. Phys. **90**(2), 1017–1025 (2001).
25. X. Yang, I. V. Kozhevnikov, Q. Huang, H. Wang, K. Sawhney, and Z. Wang, "Wideband multilayer gratings for the 17–25 nm spectral region," Opt. Express **24**(13), 15079–15092 (2016).
26. N. Benoit, S. Yulin, T. Feigl, and N. Kaiser, "Radiation stability of EUV Mo/Si multilayer mirrors," Phys. B **357**(1-2), 222–226 (2005).
27. R. van der Meer, I. V. Kozhevnikov, B. Krishnan, J. Huskens, W. van der Wiel, P. Hegeman, C. Brons, H. M. J. Bastiaens, K.-J. Boller, and F. Bijkerk, "Single-order operation of lamellar multilayer gratings in the soft x-ray spectral range," AIP Adv. **3**(1), 012103 (2013).